

Dispersion in the large-deviation regime. Part II: cellular flow at large Péclet number

P. H. Haynes¹ and J. Vanneste^{2†}

¹Department of Applied Mathematics and Theoretical Physics, University of Cambridge,
Wilberforce Road, Cambridge CB3 0WA, UK

²School of Mathematics and Maxwell Institute for Mathematical Sciences, University of
Edinburgh, King's Buildings, Edinburgh EH9 3JZ, UK

(Received 12 July 2021)

A standard model for the study of scalar dispersion through the combined effect of advection and molecular diffusion is a two-dimensional periodic flow with closed streamlines inside periodic cells. Over long time scales, the dispersion of a scalar released in this flow can be characterised by an effective diffusivity that is a factor $Pe^{1/2}$ larger than molecular diffusivity when the Péclet number Pe is large. Here we provide a more complete description of dispersion in this regime by applying the large-deviation theory developed in Part I of this paper. Specifically, we derive approximations to the rate function governing the scalar concentration at large time t by carrying out an asymptotic analysis of the relevant family of eigenvalue problems.

We identify two asymptotic regimes and, for each, make predictions for the rate function and spatial structure of the scalar. Regime I applies to distances $|\mathbf{x}|$ from the scalar release point that satisfy $|\mathbf{x}| = O(Pe^{1/4}t)$. The concentration in this regime is isotropic at large scales, is uniform along streamlines within each cell, and varies rapidly in boundary layers surrounding the separatrices between adjacent cells. The results of homogenisation theory, yielding the $O(Pe^{1/2})$ effective diffusivity, are recovered from our analysis in the limit $|\mathbf{x}| \ll Pe^{1/4}t$. Regime II applies when $|\mathbf{x}| = O(Pe t / \log Pe)$ and is characterised by an anisotropic concentration distribution that is localised around the separatrices. A novel feature of this regime is the crucial role played by the dynamics near the hyperbolic stagnation points. A consequence is that in part of the regime the dispersion can be interpreted as resulting from a random walk on the lattice of stagnation points. The two regimes overlap so that our asymptotic results describe the scalar concentration over a large range of distances $|\mathbf{x}|$. They are verified against numerical solutions of the family of eigenvalue problems yielding the rate function.

1. Introduction

The transport and mixing of constituents by fluid flows is a classical problem in fluid dynamics, motivated by a broad range of industrial and environmental applications. One of the main strands of the research on this problem, e.g. reviewed in Majda & Kramer (1999), examines how the interaction between advection and molecular diffusion leads to enhanced transport and mixing. The dispersion resulting from advection and molecular diffusion gives, in the long-time limit, both linearly increasing variance of particle positions and Gaussian concentration distributions and can therefore be quantified by means of an effective diffusivity (typically much increased compared to the molecular value). Several approaches—including homogenisation—are available to calculate this effective

† Email address for correspondence: J.Vanneste@ed.ac.uk

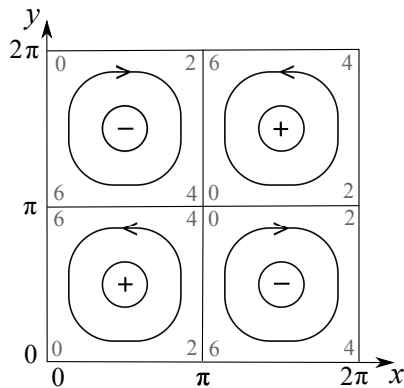


FIGURE 1. Schematic of the streamlines in single periodic cell for the flow with streamfunction (2.2). The quarter-cells with anticlockwise (clockwise) circulation are denoted by the + (−) signs. The value of the coordinate σ used in the boundary-layer analyses of §§3.2 and 4 is indicated at the corner of each quarter-cell by the grey number.

42 diffusivity and, in simple examples at least, they yield instructive closed-form results
 43 (Majda & Kramer 1999). Classical examples of this type are shear flows, originally con-
 44 sidered by Taylor (1953), and the cellular flow on which the present paper focuses. The
 45 cellular flow is a two-dimensional periodic incompressible flow, with streamfunction

$$\psi = -Ua \sin(x/a) \sin(y/a), \quad (1.1)$$

46 where U is the maximum flow speed and $2\pi a$ is the cell period. This flow consists of a
 47 doubly infinite array of periodic cells in which the fluid is rotating alternatively clock-
 48 wise and anti-clockwise as sketched in Fig. 1. It was introduced in studies of kinematic
 49 dynamos (Childress 1979) and has since become a benchmark for work on advection-
 50 diffusion (e.g. Moffatt 1983). The enhancement of dispersion by this flow (over that which
 51 results from molecular diffusion alone) is encapsulated by the results of Soward (1987),
 52 Shraiman (1987) and Rosenbluth et al. (1987) showing that the effective diffusivity in
 53 this case scales like $\text{Pe}^{1/2}$ as $\text{Pe} \rightarrow \infty$. Here

$$\text{Pe} = Ua/\kappa, \quad (1.2)$$

54 with κ the molecular diffusivity, is the Péclet number, which measures the relative
 55 strength of advection and diffusion in the flow. Several other explicit results are also
 56 available for this flow, see Majda & Kramer (1999) and references therein.

57 When applied to initial-value problems, which typically involve a passive scalar released
 58 initially in a small region, the characterisation of dispersion by a single effective diffusivity
 59 relies on an implicit assumption: the distances $|\mathbf{x}|$ between points of interest and the
 60 scalar-release region are assumed to be moderately large, specifically to be $O(t^{1/2})$ for
 61 large times t . For larger distances, the approximation by a diffusive, Gaussian process is
 62 invalid. In a companion paper (Haynes & Vanneste 2014, hereafter referred to as Part
 63 I) we show that the scalar distribution at such distances can nonetheless be described
 64 analytically, using the theory of large deviations. Part I provides a general formulation for
 65 the theory of large deviations relevant to dispersion problems and applies it to shear flows
 66 and to periodic flows including the cellular flow (1.1). The results presented there for the
 67 cellular flow are largely numerical although asymptotic expressions are obtained in the
 68 regime $\text{Pe} \ll 1$ corresponding to weak advection. In the present paper we obtain detailed
 69 asymptotic results for the opposite, and arguably more physically interesting, regime
 70 $\text{Pe} \gg 1$ corresponding to weak diffusion. In this limit, diffusion acts as a small, singular

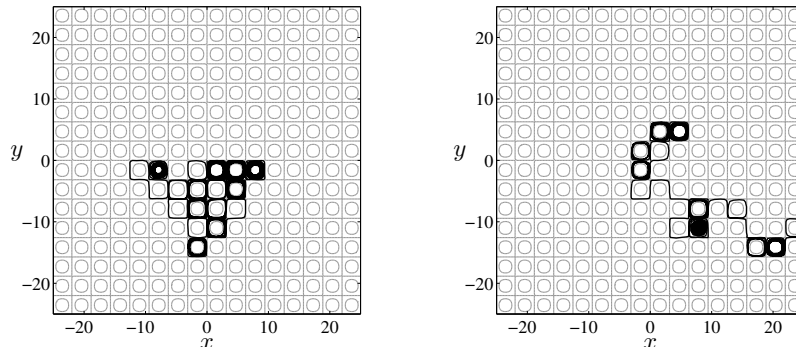


FIGURE 2. Examples of particle trajectories for $Pe = 1000$. The black lines show the trajectories $\mathbf{x}(t)$ for $0 \leq t \leq 2000$ of two particles initially released at the origin for two different realisations of the Brownian motion. The grey lines indicate the streamlines $\psi = 0$ (separatrices) and $\psi = \pm 1/2$.

71 perturbation to advection: in the complete absence of diffusion, there is no large-scale
 72 transport since particle trajectories are confined to closed streamlines inside quarter cells
 73 (see Figure 1). A weak diffusion makes it possible for particles to migrate from streamline
 74 to streamline and, when crossing the separatrices, from cell to cell, leading to large-scale
 75 transport. The importance of the separatrices is reflected in the asymptotic analysis
 76 which largely consists of a boundary-layer treatment of an $O(Pe^{-1/2})$ region surrounding
 77 them.

78 Specifically, we identify and study two asymptotic regimes, characterised by differ-
 79 ent scalings of $|\mathbf{x}|/t$ relative to Pe and leading to different asymptotic reductions. The
 80 boundary-layer analysis in the first regime turns out to be same as that appearing in
 81 the computation of the $O(Pe^{1/2})$ effective diffusivity (Childress 1979; Soward 1987), even
 82 though the regime applies over a broader range of $|\mathbf{x}|/t$ and captures non-diffusive effects.
 83 The boundary-layer analysis in the second case is novel. It requires a careful treatment
 84 of the regions around the stagnation points, leading to a logarithmic dependence of the
 85 results on Pe . Note that in both cases the asymptotic analysis is formal: we make no
 86 attempt at bounding error terms. Instead, we check our asymptotic predictions against
 87 numerical solutions of the eigenvalue problem determining the scalar concentration in
 88 the large-deviation regime, and we find excellent agreement.

89 Before entering the intricacies of this asymptotic analysis, however, it is useful to have
 90 in mind a physical picture of dispersion in the cellular flow at high Pe . Figure 5 of Part
 91 I illustrates the dispersion by displaying the evolution of the concentration of a passive
 92 scalar released in the central cell. It indicates a transition, moving away from the release
 93 region, between cells that have near-uniform concentrations near the centre and cells
 94 that are depleted at larger distances, with non-zero concentration essentially confined to
 95 the neighbourhood of the separatrices. The asymptotic analysis presented in this paper
 96 captures this transition and provides the analytic form of the concentration distribution
 97 over a broad range of distances. An alternative view of the problem considers independent
 98 particles released in the flow (1.1) and experiencing different realisations of the Brownian
 99 motion associated with diffusion. In this view, the (normalised) scalar concentration is
 100 interpreted as the particle-position probability distribution function. The motion of single
 101 particles is illustrated in Figure 2 showing two trajectory realisations. As expected, most
 102 of the time particles are trapped within quarter cells for long times; as the right panel
 103 suggests, however, large excursions are possible when the Brownian motion is such that

104 the particle remains close to the separatrix for some time. The statistics at large distances
 105 from the release point are then controlled by rare realisations of the Brownian motion
 106 for which the particle only rarely visits the cell interiors. The large-deviation theory we
 107 employ is the probabilistic tool required to capture the statistics of these rare realisations.

108 2. Formulation

109 We examine the dispersion of a passive scalar in the cellular flow with streamfunction
 110 (1.1). The concentration $C(\mathbf{x}, t)$ of a passive scalar released in this flow is governed by
 111 the advection–diffusion equation. Using a as reference length and the diffusive time scale
 112 a^2/κ as reference time, this equation takes the non-dimensional form

$$\partial_t C + \text{Pe} \mathbf{u} \cdot \nabla C = \nabla^2 C, \quad (2.1)$$

113 where $\mathbf{u} = (-\partial_y \psi, \partial_x \psi)$ and

$$\psi = -\sin x \sin y \quad (2.2)$$

114 are the dimensionless velocity and streamfunction. We consider the initial-value problem
 115 with initial condition $C(\mathbf{x}, 0) = \delta(\mathbf{x})$ so that $C(\mathbf{x}, t)$ can be interpreted as a particle-position
 116 probability density function for a particle released at the origin.

117 In Part I, we show that the concentration for $t \gg 1$ takes the large-deviation form

$$C(\mathbf{x}, t) \sim t^{-1} \phi(\mathbf{x}, \boldsymbol{\xi}) e^{-tg(\boldsymbol{\xi})}, \quad \text{where } \boldsymbol{\xi} = \mathbf{x}/t. \quad (2.3)$$

118 The Cramér or rate function $g(\boldsymbol{\xi})$ which appears in (2.3) controls the dispersion for
 119 $\mathbf{x} = O(t)$ and is our main object of interest. It can be determined as the Legendre
 120 transform of the dual function $f(\mathbf{q})$, identified as t^{-1} times the cumulant generating
 121 function $\log \mathbb{E} e^{\mathbf{q} \cdot \mathbf{X}}$ for the position \mathbf{X} of particles advected and diffused in the flow,
 122 where \mathbb{E} denotes expectation over the Brownian motion associated with diffusion. The
 123 relationship between $g(\boldsymbol{\xi})$ and $f(\mathbf{q})$ follows from the Ellis–Gärtner theorem, a key result
 124 of large-deviation theory (e.g. Ellis 1995; Dembo & Zeitouni 1998; den Hollander 2000;
 125 Touchette 2009). In turn, $f(\mathbf{q})$ is found as the principal eigenvalue of the eigenvalue
 126 problem

$$\nabla^2 \phi - (\text{Pe} \mathbf{u} + 2\mathbf{q}) \cdot \nabla \phi + (\text{Pe} \mathbf{u} \cdot \mathbf{q} + |\mathbf{q}|^2) \phi = f(\mathbf{q}) \phi, \quad (2.4)$$

127 where $\mathbf{q} = (q_1, q_2)$ is regarded as a parameter and $\phi(\mathbf{x}, \mathbf{q})$ is the eigenfunction which
 128 satisfies periodic boundary conditions.

129 The principal eigenvalue of (2.4) is guaranteed to be real, with a corresponding eigen-
 130 function ϕ that is real and sign definite (see Part I). This eigenfunction describes the
 131 spatial structure of the concentration: according to (2.3) and the relation $\mathbf{q} = \nabla_{\boldsymbol{\xi}} g$, the
 132 structure of $C(\mathbf{x}, t)$ at fixed t is locally proportional to $\phi(\mathbf{x}, \mathbf{x}t) \exp(-\mathbf{q} \cdot \mathbf{x})$. Note that
 133 the eigenvalue problem (2.4) also appears when the Floquet–Bloch theory of differential
 134 equations with periodic coefficients is applied to (2.1) (see Bensoussan et al. 1989, §4.3.1;
 135 Papanicolaou 1995, §3.6), and in the problem of front propagation in the presence of an
 136 FKPP chemical reaction (see Novikov & Ryzhik 2007; Xin 2009).

137 In Part I, we examine scalar dispersion in cellular flows by solving (2.4) numerically
 138 for fixed Pe for a range of values \mathbf{q} and then deducing $g(\boldsymbol{\xi})$ by Legendre transform.
 139 We also provide an asymptotic approximation to $f(\mathbf{q})$ in the limit $\text{Pe} \rightarrow 0$. Here we
 140 obtain a detailed description in the opposite limit $\text{Pe} \rightarrow \infty$. This limit has received
 141 a great deal of attention, most of which has been devoted to the determination of an
 142 effective diffusivity k (Childress 1979; Shraiman 1987; Rosenbluth et al. 1987; Soward
 143 1987; Fannjiang & Papanicolaou 1994; Koralov 2004; Novikov et al. 2005; Gorb et al.
 144 2011). This characterises the dispersion for $\mathbf{x} = O(t^{1/2})$ by providing the (Gaussian)

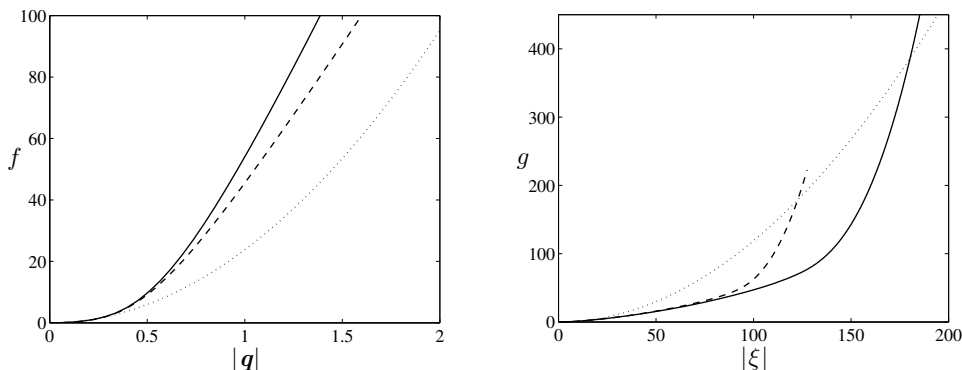


FIGURE 3. Eigenvalue $f(\mathbf{q})$ and rate function $g(\boldsymbol{\xi})$ for the cellular flow with $\text{Pe} = 250$ compared with the diffusive approximation (2.7). Left: $f(\mathbf{q})$ as a function of $|\mathbf{q}|$ for $\mathbf{q} = |\mathbf{q}|(1, 1)/\sqrt{2}$ (solid line) and $\mathbf{q} = |\mathbf{q}|(1, 0)$ (dashed line). Right: $g(\boldsymbol{\xi})$ as a function of $|\boldsymbol{\xi}|$ for $\boldsymbol{\xi} = |\boldsymbol{\xi}|(1, 1)/\sqrt{2}$ (solid line) and $\boldsymbol{\xi} = |\boldsymbol{\xi}|(1, 0)$ (dashed line). The diffusive approximation is shown by the dotted lines.

diffusive approximation $C(\mathbf{x}, t) \asymp \exp(-|\mathbf{x}|^2/(4kt))$ to the concentration. The key result in this area is the asymptotic approximation

$$k \sim 2\nu\text{Pe}^{1/2} \quad (2.5)$$

(Childress 1979; Shraiman 1987; Rosenbluth et al. 1987; Soward 1987), where the constant

$$\nu = \left(\frac{2}{\pi}\right)^{1/2} \sum_{n=0}^{\infty} \frac{(-1)^n}{(2n+1)^{1/2}} = 0.532740705 \dots \quad (2.6)$$

was determined by Soward (1987). This result is obtained by applying a boundary-layer analysis to the so-called cell problem which arises when computing an effective diffusivity using the method of homogenisation (e.g. Majda & Kramer 1999). Since the effective diffusivity can be deduced from the large-deviation functions f and g , specifically from their Taylor expansions

$$f(\mathbf{q}) \sim k|\mathbf{q}|^2 \quad \text{and} \quad g(\boldsymbol{\xi}) \sim |\boldsymbol{\xi}|^2/(4k) \quad (2.7)$$

for small \mathbf{q} or $\boldsymbol{\xi}$ (see Part I), this result is recovered in our large-deviation treatment.

To illustrate the limitations of the diffusive approximation, we show in Figure 3 the functions $f(\mathbf{q})$ and $g(\boldsymbol{\xi})$ computed by numerically along straight lines in each of the \mathbf{q} and $\boldsymbol{\xi}$ planes for $\text{Pe} = 250$ (these curves correspond to cross sections of Figure 10 in Part I). Both $f(\mathbf{q})$ and $g(\boldsymbol{\xi})$ differ strikingly from the parabolas of the diffusive approximation with: a clear anisotropy indicating faster dispersion along the diagonal in the \mathbf{x} plane than along the axes; a g that is broader than parabolic in a intermediate range of \mathbf{x} , corresponding to concentrations exponentially larger than those predicted by diffusion; and a sharp increase in g for large $\boldsymbol{\xi}$, corresponding to a localisation of the concentration. The asymptotic theory presented in this paper explains these features.

Our derivation of the asymptotic form of $f(\mathbf{q})$ for $\text{Pe} \gg 1$ relies on a boundary-layer analysis of (2.4). Compared with that leading to the effective diffusivity (2.5), this derivation is complicated by the presence of the parameter \mathbf{q} . We identify two different regimes, which we denote as I and II characterised by $|\mathbf{q}| = O(\text{Pe}^{-1/4})$ and $|\mathbf{q}| = O(1)$, respectively. Regime I is suggested by the approximation (2.5), which implies that $f(\mathbf{q}) \propto |\mathbf{q}|^2 = O(\text{Pe}^{-1/2})$ for $|\mathbf{q}| \ll 1$. In this regime, the eigenvalue $f(\mathbf{q})$ is $O(1)$ and is determined by matching a non-trivial solution in the interior of the flow cells with

170 a boundary-layer solution along the separatrices dividing the cells. The boundary-layer
 171 problem for the whole of Regime I turns out to be identical to that arising in the ho-
 172 mogenisation approach and solved by Soward (1987). However, it is only in the limit
 173 $\text{Pe}^{-1/4}|\mathbf{q}| \rightarrow 0$ that the homogenisation solution, with ϕ constant in the cell interiors,
 174 and the results (2.5)–(2.7) are recovered. In regime II, ϕ vanishes to leading order in the
 175 cell interior, and the eigenvalue problem is entirely controlled by the behaviour in the
 176 boundary layers. It turns out that $f(\mathbf{q}) = O(\text{Pe}/\log \text{Pe})$ in this case. A third regime, ex-
 177 pected to arise for $|\mathbf{q}| = O(\text{Pe})$, is not considered here since it corresponds to exceedingly
 178 small concentrations. It is commented upon the the conclusion of the paper.

179 We derive the solution $f(\mathbf{q})$ in regimes I and II in sections §§3–4. The implications for
 180 the rate function $g(\boldsymbol{\xi})$ are presented in §5; this provides a more direct physical interpre-
 181 tation of the results since $g(\boldsymbol{\xi}) \sim t^{-1} \log C(\mathbf{x}, t)$ (see Part I, §2.2, for some remarks on
 182 the qualitative links between $f(\mathbf{q})$ and $g(\boldsymbol{\xi})$). The paper concludes with a brief discussion
 183 in §6. Throughout the paper we use the following notational convention. In the period
 184 $[0, 2\pi] \times [0, 2\pi]$ of the flow, two types of quarter cells of size $\pi \times \pi$ need to be distin-
 185 guished, depending on whether the flow circulates in the positive or negative direction
 186 (see Figure 1). We denote by $+$ the first type, and by $-$ the second; when using \pm or \mp
 187 for expressions with opposite signs in the different cells, the upper (lower) sign refers to
 188 $+$ ($-$) cells (so that $\psi = \mp 1$ at the centre of cells).

189 3. Regime I: $|\mathbf{q}| = O(\text{Pe}^{-1/4})$

190 To analyse this first regime, we introduce $\tilde{\mathbf{q}} = \text{Pe}^{1/4}\mathbf{q}$ assumed to be $O(1)$ and consider
 191 separately the solution in the cell's interior and in a boundary layer around the separatri-
 192 ces. Note that the separatrices correspond to $\psi = 0$ and that, away from the stagnation
 193 points, ψ is a convenient coordinate with, for ψ small, ψ being proportional of the distance
 194 from the separatrix. As in the homogenisation problem (e.g. Childress 1979; Rosenbluth
 195 et al. 1987), the boundary-layer thickness scales like $\text{Pe}^{-1/2}$; thus the cell interior is
 196 defined by $|\psi| \gg \text{Pe}^{-1/2}$ while the boundary layer corresponds to $|\psi| = O(\text{Pe}^{-1/2})$.

197 3.1. Interior problem

198 Introducing the expansions

$$\phi = \phi_0 + \text{Pe}^{-1/4}\phi_1 + \text{Pe}^{-1/2}\phi_2 + \dots \quad \text{and} \quad f = f_0 + \text{Pe}^{-1/4}f_1 + \text{Pe}^{-1/2}f_2 + \dots \quad (3.1)$$

199 for the eigenfunction and eigenvalue into (2.4), we obtain

$$-\mathbf{u} \cdot \nabla \phi_0 = 0, \quad (3.2)$$

$$-\mathbf{u} \cdot \nabla \phi_j + \mathbf{u} \cdot \tilde{\mathbf{q}} \phi_{j-1} = 0, \quad j = 1, 2, 3, \quad (3.3)$$

$$\nabla^2 \phi_0 - \mathbf{u} \cdot \nabla \phi_4 + \mathbf{u} \cdot \tilde{\mathbf{q}} \phi_3 = f_0 \phi_0. \quad (3.4)$$

200 The solution to (3.2)–(3.3) is straightforward: it corresponds to the expansion in powers
 201 of $\text{Pe}^{-1/4}$ of $\exp(\text{Pe}^{-1/4}\tilde{\mathbf{q}} \cdot \mathbf{x})\Phi(\psi)$, where Φ is arbitrary. Thus, in each quarter-cell,

$$\sum_{j=0}^3 \text{Pe}^{-j/4} \phi_j = e^{\text{Pe}^{-1/4}\tilde{\mathbf{q}} \cdot \mathbf{x}} \sum_{j=0}^3 \text{Pe}^{-j/4} \Phi_j(\psi) + O(\text{Pe}^{-1}), \quad (3.5)$$

202 where the functions Φ_j remain to be determined. In particular,

$$\phi_0 = \Phi_0(\psi). \quad (3.6)$$

203 Therefore, to leading order, the solution is constant along streamlines, in accordance
 204 with familiar averaging results (cf. Rhines & Young 1983; Freidlin & Wentzell 1994). The

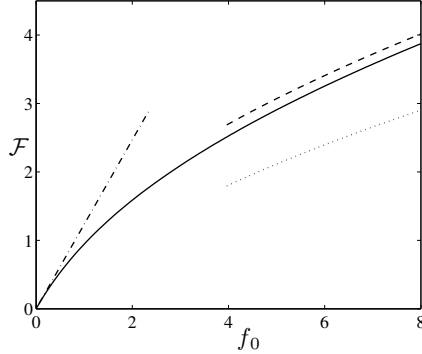


FIGURE 4. \mathcal{F} as defined by (3.10) as a function of f_0 . The numerical estimate of \mathcal{F} (solid line) is compared with asymptotic approximations for $f_0 \ll 1$ (dash-dotted line) and for $f_0 \gg 1$ (dashed line and dotted line, corresponding to two- and one-term asymptotic approximations).

higher-order terms in (3.5) are not periodic, but periodicity is restored through the rapid variation of ϕ across the boundary layer.

Eq. (3.4) can be solved for ϕ_4 provided that a solvability condition be satisfied. This solvability condition is obtained by integrating (3.4) along a streamline. Noting that the third term on the left-hand side can be written as $\mathbf{u} \cdot \tilde{\mathbf{q}} \phi_3 = \mathbf{u} \cdot \nabla(\dots)$, where \dots denotes a polynomial of degree 4 in $\tilde{\mathbf{q}} \cdot \mathbf{x}$ with ψ -dependent coefficients, this condition is found to be

$$\frac{d}{d\psi} \left(a(\psi) \frac{d\Phi_0}{d\psi} \right) = f_0 b(\psi) \Phi_0, \quad (3.7)$$

where

$$a(\psi) = 8 (E'(\psi) - \psi^2 K'(\psi)), \quad b(\psi) = 4K'(\psi), \quad (3.8)$$

and K' and E' are (complementary) complete elliptic integrals (e.g. DLMF 2010). Details of the derivation of (3.7)–(3.8) are given in Appendix A.1. Note that (3.7) can be recognised as an eigenvalue problem form of the diffusion equation obtained using averaging by Rhines & Young (1983), Freidlin & Wentzell (1994), Pauls (2006) and others.

As shown in Appendix A.1, the solution of (3.7) that is well behaved at the centres $\psi = \mp 1$ of the cell satisfies

$$\frac{d\Phi_0}{d\psi} = \pm \frac{f_0}{2} \Phi_0 \quad \text{at } \psi = \mp 1. \quad (3.9)$$

Eq. (3.7) can be solved with this boundary condition and an arbitrary normalisation to find a linear relationship between Φ_0 and its derivative near the separatrices:

$$\frac{d\Phi_0}{d\psi} \sim \pm \mathcal{F}(f_0) \Phi_0 \quad \text{as } \psi \rightarrow 0^\mp. \quad (3.10)$$

This defines the function $\mathcal{F}(f_0)$ (Dirichlet-to-Neumann map) which in practice needs to be computed numerically. The boundary-layer analysis carried out in the next section determines the value of $\mathcal{F}(f_0)$ for a given \mathbf{q} and hence gives the leading-order approximation $f_0(\mathbf{q})$ to the eigenvalue.

The form of $\mathcal{F}(f_0)$ obtained by solving (3.7)–(3.9) numerically is shown in Figure 4. Note that the fact that $\mathcal{F}(f_0)$ is positive implies that the solution decays away from the separatrices towards the centres of the cells. The asymptotic behaviour of \mathcal{F} for large

228 and small f_0 is useful. Computations detailed in Appendix A.1 give the following:

$$\mathcal{F}(f_0) \sim \frac{\pi^2 f_0}{8} \quad \text{as } f_0 \rightarrow 0, \quad (3.11)$$

$$\mathcal{F}(f_0) \sim \frac{\sqrt{2}\lambda}{4} \left(1 + \frac{\alpha}{\log \lambda} \right) \quad \text{as } f_0 \rightarrow \infty. \quad (3.12)$$

229 In (3.12), λ is a function of f_0 defined as the solution of

$$\lambda^2 = 4f_0 \log \lambda, \quad (3.13)$$

230 given explicitly in terms of a Lambert function in (A 11), and α is a constant given in
231 (A 14). The crude approximation

$$\mathcal{F}(f_0) \sim \frac{(f_0 \log f_0)^{1/2}}{2} \quad \text{as } f_0 \rightarrow \infty \quad (3.14)$$

232 is readily derived from (3.12) by neglecting the $O(\lambda/\log \lambda)$ term and using the leading-
233 order approximation $\lambda \sim (2f_0 \log f_0)^{1/2}$ to the solution of (3.13). This approximation
234 is very poor, however, with a relative error decreasing to 0 only as $1/\log(\log f_0)$. The
235 asymptotic approximations (3.11), (3.12) and (3.14) are compared with the numerical
236 solution in Figure 4. This comparison validates the approximations and shows the im-
237 portance of the logarithmic corrections to (3.14).

3.2. Boundary layer and matching

238
239 In the boundary layer surrounding the separatrices, rescaled variables need to be intro-
240 duced. Following Childress (1979), we let

$$\zeta = \mp \text{Pe}^{1/2} \psi \quad \text{and} \quad \sigma = \int_0^l |\nabla \psi| dl, \quad (3.15)$$

241 where l is the arclength along the separatrices. The sign in (3.15) is chosen such that
242 $\zeta > 0$ in the interior of the quarter-cells. As detailed in Appendix A.2, $0 < \sigma < 8$
243 parameterises the boundary of each quarter-cell, with $\sigma = 0, 2, 4, 6$ at the corners (see
244 Figure 1).

245 The eigenvalue f and eigenfunction ϕ are expanded as in (3.1), with the latter now
246 regarded as a function of ζ and σ . Introducing into (2.4) gives

$$\partial_{\zeta\zeta}^2 \phi_0 - \partial_{\sigma} \phi_0 = 0, \quad (3.16)$$

$$\partial_{\zeta\zeta}^2 \phi_1 - \partial_{\sigma} \phi_1 = -\frac{\mathbf{u} \cdot \tilde{\mathbf{q}}}{|\mathbf{u}|^2} \phi_0 \quad (3.17)$$

$$\partial_{\zeta\zeta}^2 \phi_2 - \partial_{\sigma} \phi_2 = -\frac{\mathbf{u} \cdot \tilde{\mathbf{q}}}{|\mathbf{u}|^2} \phi_1 \quad (3.18)$$

247 Eq. (3.16) has the constant solution

$$\phi_0 = \text{const.} = \Phi_0(0),$$

248 where $\Phi_0(0)$ is the limiting value of the leading-order interior solution on the separa-
249 trices. This indicates that the interior solution $\Phi_0(\psi)$ is the same in all quarter-cells.
250 The problem posed by (3.17)–(3.18) is identical to the so-called Childress problem that
251 arises in the computation of the effective diffusivity (Childress 1979). It was solved in
252 closed form by Soward (1987) using a Wiener–Hopf technique and is discussed further in

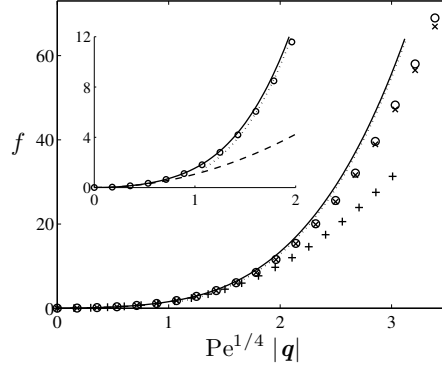


FIGURE 5. Eigenvalue $f(\mathbf{q})$ for the cellular flow as a function of $|\mathbf{q}|$ in regime I, with $\text{Pe} \gg 1$, $\text{Pe}^{1/4} \mathbf{q} = O(1)$. The asymptotic prediction (3.20) (solid line) is compared with numerical solutions of the eigenvalue problem for $\text{Pe} = 5000$ with $\mathbf{q} = |\mathbf{q}|(1, 1)/\sqrt{2}$ (\circ) and $\mathbf{q} = (|\mathbf{q}|, 0)$ (\times), and for $\text{Pe} = 500$ with $\mathbf{q} = |\mathbf{q}|(1, 1)/\sqrt{2}$ ($+$). The approximation of (3.20) valid for $\text{Pe}^{-1/4} \ll |\mathbf{q}| \ll 1$ that is deduced from (3.12) is also shown (dotted curve). The diffusive approximation (3.21), which holds for $\mathbf{q} \ll \text{Pe}^{-1/4}$, is shown in the inset magnifying the small- $|\mathbf{q}|$ region (dashed line).

253 Appendix A.2. The key result is that

$$\partial_\zeta \phi_1 \rightarrow 0 \quad \text{and} \quad \frac{\partial \phi_2}{\partial \zeta} \sim -\frac{\pi^2 \nu}{4} |\tilde{\mathbf{q}}|^2 \Phi_0(0) \quad \text{as } \zeta \rightarrow \infty, \quad (3.19)$$

254 where ν is as given in (2.6).

255 The leading-order approximation to the eigenvalue $f(\mathbf{q})$ is now obtained by matching
256 the interior and boundary solutions. Comparing (3.10) and (3.19) and taking the relation
257 between ζ and ψ (3.15) into account leads to

$$\mathcal{F}(f_0) = \frac{\pi^2 \nu}{4} |\tilde{\mathbf{q}}|^2,$$

258 and hence

$$f(\mathbf{q}) \sim \mathcal{F}^{-1} \left(\frac{\pi^2 \nu}{4} |\tilde{\mathbf{q}}|^2 \right), \quad (3.20)$$

259 where \mathcal{F}^{-1} denotes the inverse of \mathcal{F} . This is the desired approximation to the eigenvalue
260 $f(\mathbf{q})$ in regime I, with $\text{Pe}^{1/4} \mathbf{q} = O(1)$ as $\text{Pe} \rightarrow \infty$. It is completely explicit apart from the
261 requirement for numerical solution of the ODE (3.7) in order to determine \mathcal{F} . It indicates,
262 in particular, that $f(\mathbf{q})$ depends only on $|\mathbf{q}|$ in this regime, hence $g(\boldsymbol{\xi})$ depends only on
263 $|\boldsymbol{\xi}|$. Thus dispersion is isotropic not only in the diffusive regime but in the entire regime
264 I. As shown below, the anisotropy of the dispersion appears in regime II, for $\mathbf{q} \gg \text{Pe}^{-1/4}$.

265 We have verified formula (3.20) by comparison with numerical estimates of $f(\mathbf{q})$ obtained
266 by solving a discretisation of the eigenvalue problem (2.4) on a 1000^2 grid (see
267 Part I for details). The results are summarised in Figure 5. The comparison between the
268 numerical estimates obtained for different values of Pe (500 and 5000), and for different
269 orientations of \mathbf{q} (parallel to $(1, 1)$ and parallel to $(1, 0)$) confirms the dependence of f
270 on $\text{Pe}^{1/4} |\mathbf{q}|$, the isotropy of the dispersion, and more generally the validity of (3.20).

271 Formula (3.20) can be simplified further using the asymptotic approximations (3.11)
272 and (3.12) of \mathcal{F} for small and large argument. Using (3.11), (3.20) reduces to

$$f(\mathbf{q}) \sim 2\nu |\tilde{\mathbf{q}}|^2 = 2\nu \text{Pe}^{1/2} |\mathbf{q}|^2 \quad \text{for } \mathbf{q} \ll \text{Pe}^{-1/4} \quad (3.21)$$

273 This can be recognised as the diffusive approximation: the effective diffusivity deduced
274 from (2.7) recovers Soward's expression (2.5)–(2.6). On the other hand, (3.14) gives

$$f(\mathbf{q}) \sim \frac{\pi^4 \nu^2 \text{Pe} |\mathbf{q}|^4}{16 \log(\text{Pe}^{1/4} |\mathbf{q}|)} \quad \text{for } \text{Pe}^{-1/4} \ll \mathbf{q} \ll 1. \quad (3.22)$$

275 The latter approximation is poor because of the neglect of logarithmic terms, but it is
276 useful in suggesting that $f(\mathbf{q})$ is proportional to $\text{Pe}/\log \text{Pe}$ when \mathbf{q} is not small. The
277 two asymptotic approximations are shown in Figure 5. For $\tilde{\mathbf{q}} \gg 1$, we used a better
278 approximation than (3.22) obtained by inverting (3.12) numerically; this matches (3.20)
279 accurately for $|\tilde{\mathbf{q}}| \gtrsim 1$.

280 4. Regime II: $|\mathbf{q}| = O(1)$

281 In this regime, the eigenfunction vanishes to leading order in the cell interiors. The
282 problem is then entirely controlled by the behaviour inside the boundary layers around
283 the separatrices. In contrast with the situation for $|\mathbf{q}| = O(\text{Pe}^{-1/4})$, the dynamics in
284 the corners of the cells – that is, near the stagnation points – plays a crucial role. The
285 eigenvalue $f(\mathbf{q})$ scales roughly like Pe ; it is therefore convenient to introduce

$$\mathbf{f}(\mathbf{q}) = \text{Pe}^{-1} f(\mathbf{q}). \quad (4.1)$$

286 Note that $\mathbf{f}(\mathbf{q})$ is not $O(1)$ but turns out to be $O(1/\log \text{Pe})$; however, to obtain a rea-
287 sonably accurate approximation to the eigenvalue, it is important to capture logarithmic
288 corrections: in what follows we therefore treat $1/\log \text{Pe}$ as an $O(1)$ quantity and neglect
289 only terms that are algebraic in Pe^{-1} .

290 4.1. Eigenvalue problem

291 Away from the corners, the leading-order boundary-layer equation obtained from (2.4)
292 using the variables (3.15) is

$$\partial_{\zeta\zeta}^2 \phi - \partial_\sigma \phi + \frac{\mathbf{u} \cdot \mathbf{q}}{|\mathbf{u}|^2} \phi = \frac{\mathbf{f}}{|\mathbf{u}|^2} \phi, \quad (4.2)$$

293 where \mathbf{u} is evaluated on the separatrix. The solution can be written as

$$\phi = e^{\mathbf{q} \cdot \mathbf{x} + \mathbf{f}H(\sigma)} \varphi, \quad (4.3)$$

294 where

$$H(\sigma) = \frac{1}{2} \log \frac{2-\sigma}{\sigma} \quad \text{for } 0 < \sigma < 2, \quad H(\sigma+2) = H(\sigma) \quad (4.4)$$

295 and the function φ satisfies the heat equation

$$\partial_{\zeta\zeta}^2 \varphi - \partial_\sigma \varphi = 0. \quad (4.5)$$

296 See Appendix B.1 for details. Note that since ϕ is periodic, φ is not, but there is a simple
297 relation for the change in φ under a translation that represents a map from one '+' (or
298 one '-') cell to another.

299 Eq. (4.2) breaks down near the corners $\sigma = 0, 2, 4, 6$, where \mathbf{u} vanishes. There a dif-
300 ferent approximation to (2.4) needs to be considered; this provides a condition matching
301 the form of ϕ downstream of the corners to its form upstream. The analysis of the corner
302 region carried out in Appendix B.1 gives this condition as

$$\lim_{\sigma \rightarrow k^+} \varphi(\sigma, \zeta) = (16\text{Pe})^{-\mathbf{f}/2} \zeta^{\mathbf{f}} \lim_{\sigma \rightarrow k^-} \varphi(\sigma, \zeta) \quad \text{for } k = 0, 2, 4, 6. \quad (4.6)$$

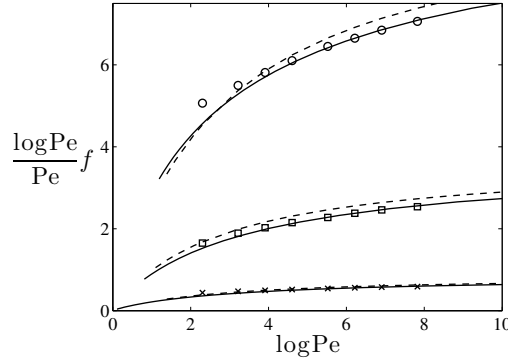


FIGURE 7. Scaled eigenvalue $f(\mathbf{q})$ as a function of Pe in regime II. The numerical solution of the eigenvalue problem (symbols) is compared with the asymptotic prediction (4.10) (solid lines) for $q_1 = q_2 = 0.5$ (\times), 1 (\square) and 2 (\circ). As $\text{Pe} \rightarrow \infty$, $\log \text{Pe} f / \text{Pe}$ slowly tends to the limiting values $2 \log \mu(\mathbf{q}, 0)$ given here by 0.85, 3.7 and 10.0. The heuristic formula (4.12) is indicated by the dashed lines.

of order $O(1/\log \text{Pe})$; it is therefore preferable to use (4.10) instead. A heuristic improvement on (4.11) retains the factor 16 inside the logarithm to read

$$f(\mathbf{q}) = \text{Pe} f(\mathbf{q}) \sim \frac{2\text{Pe}}{\log(16\text{Pe})} \log \mu(\mathbf{q}, 0). \quad (4.12)$$

In practice, we can obtain $\mu(\mathbf{q}, f)$ numerically by computing the eigenvalues of a discretised version of $\mathcal{L}(\mathbf{q}, f)$ for a range of f , then deduce the corresponding values of Pe by solving (4.10). Alternatively, if f is to be estimated for a fixed Pe , (4.10) can be solved for f iteratively, starting with (4.11). Figure 7 demonstrates the accuracy of (4.10) by comparing its prediction with the numerical solution of the full eigenvalue problem (2.4) for f for values of Pe ranging from 10 to 2500 and for three different values of $q_1 = q_2$. The figure indicates that (4.10) is useful for values of Pe as small as 100. It also confirms the limited usefulness of the leading-order asymptotics (4.11): for $q_1 = q_2 = 2$, for instance, the convergence of $\log \text{Pe} f / \text{Pe}$ to its limiting value $2 \log \mu(\mathbf{q}, 0) = 10.0$ is very slow so that exceedingly large Pe are required for an acceptable approximation. The heuristic formula (4.12), although of the same formal accuracy, provides a clear improvement.

To illustrate the validity of (4.10) over a broad range of \mathbf{q} , we compare in Figure 8 this prediction with numerical solutions along the lines $q_2 = 0$ and $q_1 = q_2$ in the \mathbf{q} -plane for $\text{Pe} = 1000$. The asymptotic prediction is virtually undistinguishable from the full numerical solution for $|\mathbf{q}| \geq 0.5$. The figure confirms the anisotropy of dispersion in regime II. A two-dimensional plot of f (see Figure 10 in Part I) indicates that the shape of constant- f contours changes from circular for small values to straight segments given by $|q_1| + |q_2| = \text{const.}$ for large values. The behaviour is confirmed explicitly in the next subsection.

4.2. Asymptotic limits

The asymptotics of $f(\mathbf{q})$ for large and small $|\mathbf{q}|$ is of interest. For simplicity, we consider the limit $|\mathbf{q}| \ll 1$ in the approximation (4.11), that is, we neglect terms that are $O(1/\log \text{Pe})$. A calculation detailed in Appendix B.2 relates the eigenvalue problem for $|\mathbf{q}| \ll 1$ to that of the $|\mathbf{q}| = O(\text{Pe}^{-1/4})$ regime and yields

$$f(\mathbf{q}) \sim \frac{\pi^4 \nu^2 \text{Pe} |\mathbf{q}|^4}{4 \log \text{Pe}}, \quad (4.13)$$

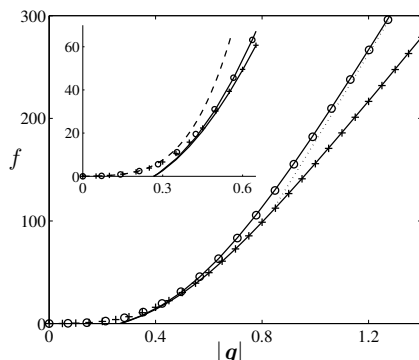


FIGURE 8. Eigenvalue $f(\mathbf{q})$ for the cellular flow for $\text{Pe} = 1000$ as a function of $|\mathbf{q}|$. The asymptotic prediction (4.10) (solid line) is compared with numerical solutions of the full eigenvalue problem (2.4) with $\mathbf{q} = |\mathbf{q}|(1, 1)/\sqrt{2}$ (\circ) and $\mathbf{q} = (|\mathbf{q}|, 0)$ ($+$). The approximation valid for $q_1, q_2 \gg 1$ that is deduced from (4.15) is also shown (dotted line). The approximation (3.20) valid for $|\mathbf{q}| = O(\text{Pe}^{-1/4})$ is shown in the inset magnifying the small- $|\mathbf{q}|$ region (dashed line).

350 which matches the limiting form (3.22) of the $|\mathbf{q}| = O(\text{Pe}^{-1/4})$ regime. This shows that
 351 regimes I and II overlap in the region $\text{Pe}^{-1/4} \ll |\mathbf{q}| \ll 1$ where $f(\mathbf{q})$ is quartic in $|\mathbf{q}|$.

352 For $|\mathbf{q}| \gg 1$, the eigenvalue problem (4.8) can be greatly simplified by retaining only
 353 the dominant elements of the matrix $\mathcal{L}(\mathbf{q}, f)$. Specifically, assuming that both $|q_1|$ and
 354 $|q_2|$ are large, the eigenvalue $\mu(\mathbf{q}, f)$ can be approximated as

$$\mu(\mathbf{q}, f) \sim e^{\pi(|q_1|+|q_2|)/2} \hat{\mu}(f), \quad (4.14)$$

355 where $\hat{\mu}(f)$ is the eigenvalue of the (\mathbf{q} -independent) scalar operator $\zeta^f \mathcal{H}_-$, with \mathcal{H}_- defined
 356 in (B8). This leads to the approximation

$$f \sim \frac{\text{Pe}}{\log(16\text{Pe})} [\pi(|q_1| + |q_2|) + 2 \log \hat{\mu}(f/\text{Pe})]. \quad (4.15)$$

357 The first term in the square brackets is asymptotically dominant, but for practical values
 358 of Pe the second term needs to be taken into account (so that (4.15) needs to be solved
 359 iteratively for f). Interestingly, (4.15) can be related to the large-deviation statistics of
 360 random walks: a random walk on a two-dimensional lattice, with steps of size $\pm a$ taken
 361 with probability $1/2$ at time intervals τ , is characterised by a large-deviation function

$$f(\mathbf{q}) = \frac{1}{\tau} \log(\cosh(q_1 a) \cosh(q_2 a)) \sim \frac{a}{\tau} (|q_1| + |q_2|) \quad \text{as } |\mathbf{q}| \rightarrow \infty,$$

362 assuming independent walks in the x - and y -directions. Comparison with (4.15) shows
 363 that for large Pe and large $|\mathbf{q}|$, the dispersion by a cellular flow is equivalent to a random
 364 walk on the lattice of the hyperbolic stagnation points, with time intervals $\tau \propto \log \text{Pe}/\text{Pe}$
 365 between the steps. This scaling is natural: $\text{Pe}/\log \text{Pe}$ is the time scale for both approach-
 366 ing the hyperbolic stagnation points along their stable manifold and for escaping from
 367 their neighbourhood along their unstable manifold (as consideration of the simple one-
 368 dimensional problems $dX = \mp \text{Pe} \sin X dt + \sqrt{2} dW$ readily confirms.) The physical inter-
 369 pretation is straightforward: since large values of \mathbf{q} correspond to large distances, $f(\mathbf{q})$
 370 then describes the dispersion statistics of rare particles which travel anomalously fast
 371 away from their point of release. As Figure 2 suggests, such particles move rapidly by
 372 remaining near the separatrices. The $O(\log \text{Pe}/\text{Pe})$ time they take to pass through the
 373 regions surrounding stagnation points is asymptotically larger than the $O(1/\text{Pe})$ time

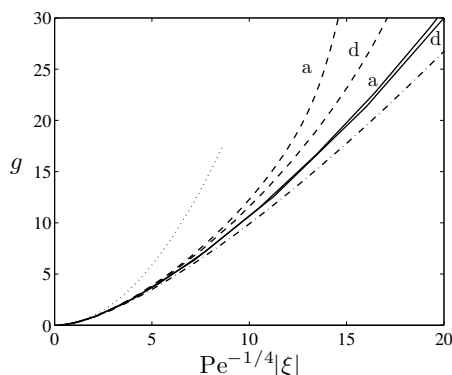


FIGURE 9. Rate function $g(\boldsymbol{\xi})$ as a function of $\text{Pe}^{-1/4}|\boldsymbol{\xi}|$ for $\text{Pe} = 100$ (dashed lines) and $\text{Pe} = 500$ (solid lines). Numerical estimates for $\boldsymbol{x} = |\boldsymbol{\xi}|(1, 1)/\sqrt{2}$ (labelled by ‘d’ for diagonal) and for $\boldsymbol{\xi} = |\boldsymbol{\xi}|(1, 0)$ (labelled by ‘a’ for axis) are compared with the asymptotic approximation (5.1) (dash-dotted line). The quadratic diffusive approximation (2.7) is also shown (dotted line).

374 spent along the separatrix between these passages. From the current stagnation point
 375 a particle may move along the unstable manifold to one of the two connected stagna-
 376 tion points. As a result, the dynamics is approximated by that of a random walk with
 377 instantaneous jumps between neighbouring stagnation points.

378 Figure 8 confirms the asymptotics (4.15) by comparing its prediction with a numerical
 379 estimate for $f(\boldsymbol{q})$ for $\text{Pe} = 1000$ and $q_1 = q_2$. The asymptotics is accurate for $q_1 = q_2 \gtrsim 1$,
 380 not surprisingly perhaps since the large parameter is in fact $\min(\exp(\pi q_1), \exp(\pi q_2))$ (see
 381 B.2). The asymptotics does not apply in the case $q_2 = 0$ also shown in the Figure and
 382 more generally if either q_1 or q_2 is $O(1)$; it is not difficult to obtain a simplified formula
 383 for this case, but this requires the eigenvalue of an operator more complicated than $\zeta^f \mathcal{H}_-$.
 384 Figure 8 also illustrates the switchover between regime I and regime II that occurs in the
 385 range $\text{Pe}^{-1/4} \ll |\boldsymbol{q}| \ll 1$ where the approximations (3.20) and (4.10) are both valid and
 386 overlap.

387 We emphasise that the validity of the approximation given here for $|\boldsymbol{q}| \gg 1$ is limited:
 388 for $|\boldsymbol{q}| = O(\text{Pe})$ or larger, terms of (2.4) that are neglected in our boundary-layer treat-
 389 ment, most obviously the term $|\boldsymbol{q}|^2 \phi$, become important. For $|\boldsymbol{q}| \gg 1$ this term dominates
 390 so that $f(\boldsymbol{q}) \sim |\boldsymbol{q}|^2$, corresponding to a purely diffusive behaviour. Physically, this de-
 391 scribes the statistics of particles that are so far from their release point that advection,
 392 with the limits imposed by the finite velocity, can no longer be the dominant mechanism
 393 of dispersion. The transition between our regime II and this diffusion-dominated regime
 394 can be expected to take place in a third regime such that $|\boldsymbol{q}| = O(\text{Pe})$ (up to logarithmic
 395 corrections); we leave the study of this regime for future work.

396 5. Rate function

397 In this section, we express the asymptotic results of §§3–4 in terms of the rate function
 398 $g(\boldsymbol{\xi})$. This is straightforward, since it only involves taking the Legendre transform of the
 399 (semi-)analytic formulas obtained for $f(\boldsymbol{q})$; it is useful however because, according to
 400 (2.3), the rate function directly provides the form of the scalar concentration.

401 The two regimes I and II identified for $f(\boldsymbol{q})$ naturally have counterparts for $g(\boldsymbol{\xi})$.
 402 Regime I, which assumes $\boldsymbol{q} = O(\text{Pe}^{-1/4})$, is valid for $|\boldsymbol{q}| \ll 1$ and yields $f(\boldsymbol{q}) = O(1)$, is
 403 readily seen to correspond to $\boldsymbol{\xi} = O(\text{Pe}^{1/4})$ and hold for $|\boldsymbol{\xi}| \ll \text{Pe}/\log \text{Pe}$. The Legendre

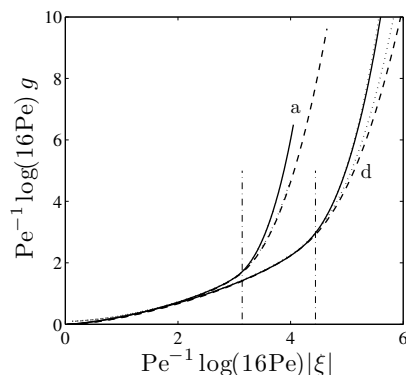


FIGURE 10. Rate function $g(\boldsymbol{\xi})$ in the scaling of Regime II for for $Pe = 100$ (dashed lines) and $Pe = 500$ (solid lines). Numerical estimates for $\boldsymbol{x} = |\boldsymbol{\xi}|(1, 1)/\sqrt{2}$ (labelled by ‘d’ for diagonal) and for $\boldsymbol{\xi} = |\boldsymbol{\xi}|(1, 0)$ (labelled by ‘a’ for axis) are compared with the asymptotic approximation derived from (4.10) (dotted line, shown for $\boldsymbol{\xi}$ along the diagonal only). The dash-dotted vertical segments indicate the vertical asymptotes (5.3) predicted for $Pe \rightarrow \infty$.

404 transform of (3.20) corresponds to a rate function of the form

$$g(\boldsymbol{\xi}) \sim \mathcal{G}(Pe^{-1/4}|\boldsymbol{\xi}|), \quad (5.1)$$

405 where the function \mathcal{G} , essentially the Legendre transform of \mathcal{F}^{-1} in (3.20) can be com-
 406 puted numerically. This prediction is verified in Figure 9 which shows $g(\boldsymbol{\xi})$ as a function
 407 of the scaled variable $Pe^{-1/4}|\boldsymbol{\xi}|$ for $Pe = 100$ and 500 and two different orientations of
 408 $\boldsymbol{\xi}$. As predicted, for $Pe^{-1/4}|\boldsymbol{\xi}|$ not too large, the curves obtained by numerical solution
 409 of the eigenvalue problem collapse and match that obtained from the asymptotic solu-
 410 tion. The diffusive approximation, with the quadratic g given in (2.7), is also shown. The
 411 physical implications of the results for regime I derived from $f(\boldsymbol{q})$ can be reiterated based
 412 on the form of $g(\boldsymbol{\xi})$: dispersion is isotropic in regime I, and the diffusive approximation
 413 considerably underestimates the dispersion, with $g(\boldsymbol{\xi})$ much flatter than quadratic away
 414 from $|\boldsymbol{\xi}| \ll Pe^{1/4}$, corresponding to exponentially higher concentrations than predicted
 415 by the effective diffusivity. The spatial distribution of the passive-scalar concentration,
 416 governed by the eigenfunction $\phi(\boldsymbol{x}, \boldsymbol{\xi})$, is shown in Part I: in regime I, the concentration
 417 has a non-trivial distribution in the cell interior with similar values in the boundary layer
 418 around the separatrices. As $\boldsymbol{\xi}$ increases from 0, the interior concentration changes from
 419 near uniform to almost zero, with the boundary layer containing essentially all the scalar
 420 for $|\boldsymbol{\xi}| \gg Pe^{1/4}$.

421 The scaling of $g(\boldsymbol{\xi})$ in regime II can be obtained from (4.12) with the caveat that neglect
 422 of some logarithmic terms limits the accuracy of the expression derived in this manner.
 423 The orders of magnitude $\boldsymbol{q} = O(1)$ and $f(\boldsymbol{q}) = O(Pe/\log Pe)$ associated with regime II
 424 correspond to $\boldsymbol{\xi} = O(Pe/\log Pe)$ and $g(\boldsymbol{\xi}) = O(Pe/\log Pe)$. More specifically, it follows
 425 from (4.12) that the rate function has the form

$$g(\boldsymbol{\xi}) \sim \frac{Pe}{\log(16Pe)} \tilde{\mathcal{G}}\left(\frac{\log(16Pe)}{Pe} \boldsymbol{\xi}\right) \quad (5.2)$$

426 for some function $\tilde{\mathcal{G}}$ deduced from $\mu(\boldsymbol{q}, 0)$. As (4.12) itself this is an asymptotically
 427 inconsistent expression, taking into account the factor 16 inside the logarithms while
 428 neglecting other terms of the same, $O(1/\log Pe)$ order. (The rate function deduced from
 429 f obtained by solving (4.10) gives a better approximation, but it is transcendental in

the Péclet number.) Figure 10 illustrates the behaviour of g in regime II by showing the same numerical results as in Figure 9 but with g and $\boldsymbol{\xi}$ scaled according to (5.2). For $\text{Pe}^{-1} \log(16\text{Pe}) \lesssim 1$, the pairs of curves corresponding to the same $\boldsymbol{\xi}$ but different Péclet numbers (100 and 500) collapse, consistent with (5.2). For somewhat larger $\boldsymbol{\xi}$, the logarithmic corrections neglected matter, and the approximation derived from (4.10) then provides the required approximation.

The most striking feature in the behaviour of $g(\boldsymbol{\xi})$ is the abrupt increase once $|\boldsymbol{\xi}|$ exceeds a certain threshold. This implies that the concentration of a passive scalar drops suddenly for distances larger than t times this threshold and, in practice, means that scalar is effectively localised to a finite support. This feature is captured by expression (4.15) which provides an approximation of $f(\mathbf{q})$ for large \mathbf{q} . Ignoring the correction term involving $\hat{\mu}(f/\text{Pe})$, the Legendre transform of (4.15) implies that

$$g(\boldsymbol{\xi}) \rightarrow \infty \quad \text{as} \quad \max(|\xi_1|, |\xi_2|) \rightarrow \xi_* = \frac{\pi\text{Pe}}{\log(16\text{Pe})}. \quad (5.3)$$

This provides an approximation for the size (and square shape) of this finite support for $\text{Pe} \rightarrow \infty$. The finite support is entirely as expected for random walks with finite jumps separated by finite time intervals (e.g. Keller 2004) which, as we have argued above, applies in the large Pe regime. For large-but-finite Pe, the increase of $g(\boldsymbol{\xi})$ with $|\boldsymbol{\xi}|$ is in fact smooth; it is encoded in $\hat{\mu}(f/\text{Pe})$ and for $|\xi_1|$ or $|\xi_2|$ substantially larger than ξ_* , by the form of $f(\mathbf{q})$ in the third regime $\mathbf{q} = O(\text{Pe})$. However, the scalar concentrations corresponding such values of $\boldsymbol{\xi}$ (that is, such distances to the scalar-release point) are very small indeed.

6. Conclusion

The large-deviation approach developed in Part I and extended here makes it possible to capture the tails in the distribution of a passive scalar released in the cellular flow (1.1). It goes much further than the homogenisation approach classically applied to this problem: while homogenisation describes only the Gaussian core of the scalar distribution characterised by $|\mathbf{x}| = O(t^{1/2})$, the large-deviation approach gives the prediction of a dependence in $\exp(-tg(\mathbf{x}/t))$ valid for much larger distances $|\mathbf{x}| = O(t)$. It furthermore provides a method for determining the rate function g by solving a family of eigenvalue problems.

The asymptotic analysis of these eigenvalue problems in the large-Péclet-number limit reveals two distinct regimes in the dispersion. It is useful to summarise the predictions in these regimes using dimensional variables. Regime I holds for moderately large distances from the release point, specifically distances that satisfy $|\mathbf{x}| \ll Ut/\log \text{Pe}$. It is characterised by an isotropic concentration that is broader than Gaussian and is controlled by the exchanges between the cell interiors across the separatrix regions. Regime II holds for $(\kappa^3 U/a^3)^{1/4} t \ll |\mathbf{x}| = O(Ut/\log \text{Pe}) \ll Ut$, is anisotropic and characterised by a sharp decrease of the concentration when $\max(|x|, |y|)$ approaches the specific value $\pi Ut/\log(16\text{Pe})$. Regime II describes the statistics of particles that remain near the separatrix at all times. The main factor limiting the concentration is then the passage through the stagnation points; near the sharp concentration decrease, the evolution is analogous to that of a random walk on the lattice formed by the stagnation points. For distances larger still, the concentration is exceedingly small and controlled by a different physical process in which molecular diffusion plays a key part; we do not analyse the corresponding regime III in this paper.

While this paper is entirely devoted to dispersion of passive scalars, the results are also

475 relevant to problems involving reacting scalars. Specifically, the speed of propagation of
 476 fronts in models such as the FKPP equation turns out to be controlled by the large-
 477 deviation rate function $g(\boldsymbol{\xi})$ for the corresponding passive-scalar problem (Gärtner &
 478 Freidlin 1979; Freidlin 1985). Thus the asymptotic results of this paper can serve as a
 479 basis for new predictions for the propagation speed of fronts in cellular flows as studied,
 480 e.g., by Abel et al. (2002) and Novikov & Ryzhik (2007). These predictions are presented
 481 in papers by Tzella & Vanneste (2014*a,b*); these also discuss regime III which turns out
 482 to be important for large reaction rates.

483 We conclude by noting that the form of the large-deviation theory used in this paper is
 484 an additive one, in the sense that it applies to SDEs with additive noise (and is therefore
 485 very close to Cramér’s original theory for the sum of random numbers). Its multiplicative
 486 counterpart, exemplified by SDEs with multiplicative noise, is also relevant to the passive-
 487 scalar problem. It applies to the finite-time Lyapunov exponents which measure the rate
 488 of stretching experienced by line elements in a flow: for sufficiently mixing flows, their
 489 statistics obey a large-deviation principle and, remarkably, there is a significant part of
 490 parameter space in which the corresponding rate function controls the decay rate of the
 491 variance of passive scalars in such flows (e.g. Tsang et al. 2005; Haynes & Vanneste 2005).

492 **Acknowledgments.** The authors thank A. Tzella for useful discussions. JV acknowl-
 493 edges support from grant EP/I028072/1 from the UK Engineering and Physical Sciences
 494 Research Council.

495 Appendix A. Derivation details for $|q| = O(\text{Pe}^{-1/4})$

496 A.1. Interior solution

497 We obtain the solvability condition (3.7) by integrating (3.4) along streamlines. To do
 498 this, we introduce the time-like coordinate s such that

$$\frac{d}{ds} = \mathbf{u} \cdot \nabla, \quad \text{i.e.} \quad ds = \frac{dx}{\sin x \cos y} = -\frac{dy}{\cos x \sin y}, \quad (\text{A } 1)$$

499 that is used in conjunction with the value of the streamfunction ψ . We first note that

$$\oint (\mathbf{u} \cdot \nabla \phi_4 + (\mathbf{u} \cdot \bar{\mathbf{q}}) \phi_3) ds = 0,$$

500 where the integration is along a streamline, can be deduced from (3.5), specifically that
 501 ϕ_3 is a sum of products of functions of $\bar{\mathbf{q}} \cdot \mathbf{x}$ and functions of ψ , and that fact that
 502 $\oint \mathbf{u} \cdot \nabla f(\mathbf{x}) ds = 0$ for any function $f(\mathbf{x})$. Integrating (3.4) along a streamline then gives

$$\oint \nabla^2 \phi_0 ds = f_0 \oint \phi_0 ds. \quad (\text{A } 2)$$

503 Now, following Rhines & Young (1983), we use the arclength $dl = |\nabla \psi| ds$ to compute

$$\oint \nabla^2 \phi_0 ds = \frac{d}{d\psi} \iint \nabla^2 \phi_0 dx dy = \frac{d}{d\psi} \oint \nabla \phi_0 \cdot d\mathbf{l} = \frac{d}{d\psi} \left(\oint |\nabla \psi| dl \frac{d\phi_0}{d\psi} \right)$$

504 and reduce (A 2) to the form (3.7), where

$$a(\psi) = \oint |\nabla \psi| dl = \oint |\nabla \psi|^2 ds \quad \text{and} \quad b(\psi) = \oint \frac{dl}{|\nabla \psi|} = \oint ds \quad (\text{A } 3)$$

505 can be recognised respectively as the circulation and the orbiting time around streamlines.

506 The explicit expressions (3.8) for $a(\psi)$ and $b(\psi)$ are obtained as follows. To compute

507 $b(\psi)$, we eliminate y from (A 1) using the constancy of $\psi = -\sin x \sin y$ and compute

$$b(\psi) = 2 \int_{\sin^{-1} \psi}^{\pi - \sin^{-1} \psi} \frac{dx}{\sqrt{\sin^2 x - \psi^2}} = 4K'(\psi),$$

508 where $K'(\psi) = K(\sqrt{1 - \psi^2})$ is a complete elliptic integral of the first kind (DLMF 2010),
509 and we have temporarily assumed that $0 \leq \psi \leq 1$. For $a(\psi)$, we observe that

$$a(\psi) = \iint \nabla^2 \psi \, dx dy = -2 \iint \psi \, d\psi ds = -2 \int \psi d\psi \oint ds = -2 \int \psi b(\psi) \, d\psi,$$

510 and hence that

$$\frac{da}{d\psi} = -2\psi b(\psi).$$

511 This equation can be integrated: using formula (19.4.2) in DLMF (2010) we obtain

$$a(\psi) = 8 (E'(\psi) - \psi^2 K'(\psi)),$$

512 where $E'(\psi) = E(\sqrt{1 - \psi^2})$ is a complete elliptic integral of the second kind.

513 The following properties of $a(\psi)$ and $b(\psi)$ are useful:

$$a(0) = 8, \quad b(\psi) \sim 4 \log(4/|\psi|) \quad \text{as } \psi \rightarrow 0, \quad (\text{A } 4)$$

$$a(\psi) \sim 4\pi(1 \pm \psi) \quad \text{as } \psi \rightarrow \mp 1, \quad b(\mp 1) = 2\pi. \quad (\text{A } 5)$$

514 In particular, using (A 5), a Frobenius expansion shows that solutions of (3.7) bounded
515 at $\psi = \mp 1$ have the form

$$\Phi_0 = C(1 + f_0(1 \pm \psi)/2 + O((1 \pm \psi)^2)),$$

516 where C in arbitrary constant (the other solutions have a logarithmic singularity). This
517 leads to the boundary condition (3.9).

518 We now consider the solution of (3.7) in the limits $f_0 \rightarrow 0$ and $f_0 \rightarrow \infty$ and derive the
519 asymptotic expressions (3.11)–(3.12) for $\mathcal{F}(f_0)$. For $f_0 \rightarrow 0$, $\Phi_0 = 1 + O(f_0)$; introducing
520 this in the right-hand side of (3.7), integrating and imposing boundedness gives

$$\frac{d\Phi_0}{d\psi} \sim \frac{f_0}{a(\psi)} \int_{\pm 1}^{\psi} b(\psi') \, d\psi'$$

521 and hence

$$\mathcal{F}(f_0) \sim \frac{f_0}{a(0)} \int_0^1 b(\psi) \, d\psi = \frac{\pi^2 f_0}{8}.$$

522 For $f_0 \rightarrow \infty$, it is convenient to introduce

$$r(\psi) = \frac{a(\psi)}{\Phi_0(\psi)} \frac{d\Phi_0}{d\psi} \quad (\text{A } 6)$$

523 which satisfies the Riccati equation

$$\frac{dr}{d\psi} = f_0 b(\psi) - \frac{r^2}{a(\psi)}. \quad (\text{A } 7)$$

524 The solutions of interest decay with $|\psi|$ and are approximated by

$$r = \pm (f_0 a(\psi) b(\psi))^{1/2}$$

525 away from $\psi = 0$. (A boundary layer of $O(f_0^{-1})$ width appears around the centres $\psi = \mp 1$
526 so that the boundary condition (3.9) can be satisfied.)

527 Near $\psi = 0$, (A 7) is approximated as

$$\frac{dr}{d\psi} = 4f_0 \log(4/|\psi|) - \frac{1}{8}r^2 + O(f_0\psi^2). \quad (\text{A } 8)$$

528 using (A 4). A dominant-balance argument suggests to introduce

$$\Psi = \lambda\psi \quad \text{and} \quad R = r/\lambda, \quad (\text{A } 9)$$

529 where λ satisfies

$$\lambda^2 = 4f_0 \log \lambda \quad (\text{A } 10)$$

530 Note that this equation has the closed-form solution

$$\lambda = \exp\left(-\frac{W_m(-1/(2f_0))}{2}\right) \quad (\text{A } 11)$$

531 in terms of the Lambert function W_m (e.g. DLMF 2010), and the approximate solution

$$\lambda \sim (2f_0 \log f_0)^{1/2} \quad \text{as } f_0 \rightarrow \infty.$$

532 Introducing (A 9) transforms (A 8) into

$$\frac{dR}{d\Psi} = 1 - \frac{R^2}{8} + \frac{\log(4/|\Psi|)}{\log \lambda} + O(1/(\lambda \log \lambda)), \quad (\text{A } 12)$$

533 where we assume $\Psi = O(1)$. We solve this equation perturbatively: the expansion

$$R = \pm 2\sqrt{2} + \frac{R_1}{\log \lambda} + O(1/(\lambda \log \lambda)), \quad (\text{A } 13)$$

534 where $R_1(\psi)$ remains to be determined, satisfies (A 12) to leading order. At the next
535 order, we find

$$\frac{dR_1}{d\Psi} = \pm \frac{\sqrt{2}}{2} R_1 + \log \frac{4}{|\Psi|}.$$

536 The solution that is bounded as $|\Psi| \rightarrow \infty$ takes the form

$$R_1 = \mp \sqrt{2} \log(|\Psi|/4) \mp \sqrt{2} e^{\sqrt{2}|\Psi|/2} \text{Ei}(\sqrt{2}|\Psi|/2),$$

537 where Ei is the exponential integral (e.g. DLMF 2010). Evaluating at $\Psi = 0$ gives

$$R_1(0) = \pm \frac{\sqrt{2}}{2} (3 \log 2 + 2\gamma),$$

538 where γ is Euler's constant. After introducing this result into (A 13), we find from (A 9),
539 (A 6) and (A 4) that

$$\mathcal{F}(f_0) \sim \frac{\sqrt{2}\lambda}{4} \left(1 + \frac{\alpha}{\log \lambda}\right), \quad \text{where } \alpha = \frac{3 \log 2 + 2\gamma}{4} = 0.8084682178 \dots \quad (\text{A } 14)$$

540 A.2. Boundary-layer solution

541 The boundary layer equations (3.17)–(3.18) are essentially identical to those to be solved
542 to compute the effective diffusivity using a homogenisation approach. Thus the solution
543 follows closely Childress (1979) and Soward (1987) and is detailed here for completeness
544 (see also Childress & Soward 1989).

545 Since the solution is identical in the quarter-cells with the same sense of flow rotation,
546 we concentrate on the + quarter-cell $[0, \pi] \times [0, \pi]$ and on the – cell $[0, \pi] \times [\pi, 2\pi]$. We

547 note that

$$\begin{aligned} 0 < \sigma = 1 - \cos x < 2 \quad \text{for } y = 0, \quad 2 < \sigma = 3 - \cos y < 4 \quad \text{for } x = \pi, \\ 4 < \sigma = 5 + \cos x < 6 \quad \text{for } y = \pi, \quad 6 < \sigma = 7 + \cos y < 8 \quad \text{for } x = 0. \end{aligned}$$

548 in the + quarter-cell, while

$$\begin{aligned} 0 < \sigma = 1 - \cos x < 2 \quad \text{for } y = 2\pi, \quad 2 < \sigma = 3 - \cos y < 4 \quad \text{for } x = \pi, \\ 4 < \sigma = 5 + \cos x < 6 \quad \text{for } y = \pi, \quad 6 < \sigma = 7 + \cos y < 8 \quad \text{for } x = 0. \end{aligned}$$

549 in the - quarter-cell. Eqs. (3.17)–(3.18) are solved in these two quarter-cells. This leads
550 to solutions $\phi_k^\pm(\sigma, \zeta)$, $k = 1, 2$, that need to be matched across the separatrix $\zeta = 0$.
551 Using periodicity, the matching conditions are found to be

$$\begin{aligned} \phi_k^+(\sigma, 0) = \phi_k^-(\sigma, 0) \quad \text{and} \quad \partial_\zeta \phi_k^+(\sigma, 0) = -\partial_\zeta \phi_k^-(\sigma, 0) \quad \text{for } 0 < \sigma < 2, \quad 4 < \sigma < 6, \\ \phi_k^+(\sigma, 0) = \phi_k^-(\sigma + 4, 0) \quad \text{and} \quad \partial_\zeta \phi_k^+(\sigma, 0) = -\partial_\zeta \phi_k^-(\sigma + 4, 0) \quad \text{for } 2 < \sigma < 4, \quad 6 < \sigma < 8, \end{aligned}$$

552 with the ϕ_k^\pm periodic with period 8 (see Fig. 1).

553 Using that $\phi_0 = \Phi_0(0)$ is a constant, (3.17) is written explicitly as

$$\partial_{\zeta\zeta}^2 \phi_1^\pm - \partial_\sigma \phi_1^\pm = -\tilde{q}_1 F(\sigma) \mp \tilde{q}_2 F(\sigma - 2), \quad (\text{A 15})$$

554 where

$$F(\sigma) = \begin{cases} (2\sigma - \sigma^2)^{-1/2} & \text{for } 0 < \sigma < 2 \\ 0 & \text{for } 2 < \sigma < 4 \end{cases} \quad \text{and} \quad F(\sigma + 4) = -F(\sigma). \quad (\text{A 16})$$

555 For convenience, we have used the linearity of (3.17)–(3.18) to set $\phi_0 = \Phi_0(0) = 1$
556 temporarily.

557 It follows from (A 15)–(A 16) that $\phi_1^\pm(\sigma + 4, \zeta) = -\phi_1^\pm(\sigma, \zeta)$ and so the matching
558 conditions become

$$\phi_1^+(\sigma, 0) = \phi_1^-(\sigma, 0) \quad \text{and} \quad \partial_\zeta \phi_1^+(\sigma, 0) = -\partial_\zeta \phi_1^-(\sigma, 0) \quad \text{for } 0 < \sigma < 2, \quad 4 < \sigma < 6, \quad (\text{A 17})$$

$$\phi_1^+(\sigma, 0) = -\phi_1^-(\sigma, 0) \quad \text{and} \quad \partial_\zeta \phi_1^+(\sigma, 0) = \partial_\zeta \phi_1^-(\sigma, 0) \quad \text{for } 2 < \sigma < 4, \quad 6 < \sigma < 8, \quad (\text{A 18})$$

559 Defining $G(\sigma)$ by

$$G'(\sigma) = F(\sigma) \quad \text{and} \quad \int_0^8 G(\sigma) d\sigma = 0, \quad (\text{A 19})$$

560 that is,

$$G(\sigma) = \begin{cases} \sin^{-1}(\sigma - 1) & \text{for } 0 < \sigma < 2, \\ \pi/2 & \text{for } 2 < \sigma < 4 \end{cases}, \quad G(\sigma + 4) = -G(\sigma),$$

561 the solution to (A 15)–(A 18) can be written as

$$\phi_1^\pm(\sigma, \zeta) = \tilde{q}_1 (G(\sigma) + \varrho(\sigma, \zeta)) \pm \tilde{q}_2 (G(\sigma - 2) + \varrho(\sigma - 2, \zeta)), \quad (\text{A 20})$$

562 where $\varrho(\sigma, \zeta)$ satisfies

$$\begin{aligned} \partial_{\zeta\zeta}^2 \varrho - \partial_\sigma \varrho = 0, \quad \partial_\zeta \varrho(\sigma, 0) = 0 \quad \text{for } 0 < \sigma < 2, \quad 4 < \sigma < 6, \\ \varrho(\sigma, 0) = -G(\sigma) \quad \text{for } 2 < \sigma < 4, \quad 6 < \sigma < 8. \end{aligned}$$

563 Since $G(\sigma) = \pi/2$ for $2 < \sigma < 4$ and $G(\sigma) = -\pi/2$ for $6 < \sigma < 8$,

$$\varrho(\sigma, \zeta) = -\frac{\pi}{2} \theta(\sigma + 2, \zeta), \quad (\text{A 21})$$

564 where $\theta(\sigma, \zeta)$ satisfies

$$\begin{aligned} \partial_{\zeta}^2 \theta - \partial_{\sigma} \theta &= 0, \quad \theta(\sigma, 0) = -1 \quad \text{for } 0 < \sigma < 2, \\ \theta(\sigma, 0) &= 1 \quad \text{for } 4 < \sigma < 6, \\ \partial_{\zeta} \theta(\sigma, 0) &= 0 \quad \text{for } 2 < \sigma < 4, \quad 6 < \sigma < 8, \end{aligned}$$

565 with $\theta \rightarrow 0$ as $\zeta \rightarrow \infty$. This is the problem solved in closed form by Soward (1987) using
566 a Wiener–Hopf technique.

567 The solution (A 20) can now be introduced into Eq. (3.18) satisfied by ϕ_2 in order to
568 obtain $\partial_{\zeta} \phi_2$ as $\zeta \rightarrow \infty$. We first rewrite (3.18) as

$$\partial_{\zeta}^2 \phi_2^{\pm} - \partial_{\sigma} \phi_2^{\pm} = -[\tilde{q}_1 F(\sigma) \pm \tilde{q}_2 F(\sigma - 2)] \phi_1^{\pm}, \quad (\text{A } 22)$$

569 and note that the leading-order behaviour of the solution as $\zeta \rightarrow \infty$ is controlled by the
570 average in σ :

$$\phi_2^{\pm} \sim \bar{\phi}_2^{\pm} = \frac{1}{8} \int_0^8 \phi_2^{\pm} d\sigma \quad \text{as } \zeta \rightarrow \infty.$$

571 Introducing (A 20) into the average of (A 22) and using (A 19) and symmetries reduces
572 this equation to

$$\partial_{\zeta}^2 \bar{\phi}_2^{\pm} = -\frac{|\tilde{\mathbf{q}}|^2}{4} \int_0^2 F(\sigma) \varrho(\sigma, \zeta) d\sigma.$$

573 Integrating with respect to ζ then gives

$$\partial_{\zeta} \bar{\phi}_2^{\pm} = -\frac{|\tilde{\mathbf{q}}|^2}{4} \int_0^2 F(\sigma) \int_0^{\infty} \varrho(\sigma, \zeta) d\zeta d\sigma = -\frac{\pi |\tilde{\mathbf{q}}|^2}{4} \int_0^{\infty} \varrho(0, \zeta) d\zeta,$$

574 on using that $\partial_{\sigma} \int_0^{\infty} \varrho(\sigma, \zeta) d\zeta = -\partial_{\zeta} \varrho(\sigma, 0) = 0$ for $0 < \sigma < 2$. We finally obtain (3.19)
575 using (A 21) above and formula (A.9) in Soward (1987), namely

$$\int_0^{\infty} \theta(2, \zeta) d\zeta = -2\nu,$$

576 where ν is defined by (2.6).

577 Appendix B. Derivation details for $|\mathbf{q}| = O(1)$

578 B.1. Boundary-layer solution

579 To solve (4.2), we note that $\partial_{\sigma}(\cdot) = \mathbf{u} \cdot \nabla(\cdot)/|\mathbf{u}|^2$, hence $\partial_{\sigma} \mathbf{x} = \mathbf{u}/|\mathbf{u}|^2$, and that $H(\sigma)$
580 defined in (4.4) satisfies

$$H(\sigma) = -\int_1^{\sigma} F^2(\sigma') d\sigma' = -\int_1^{\sigma} \frac{d\sigma'}{|\mathbf{u}(\sigma')|^2}.$$

581 The undifferentiated terms in (4.2) can therefore be integrated explicitly to obtain (4.3)–
582 (4.5). The periodicity of ϕ and the symmetry of the system imply the relationships

$$\varphi(x + k\pi, y + l\pi) = e^{-\pi(kq_1 + lq_2)} \varphi(x, y), \quad (\text{B } 1)$$

583 for all integers k, l with $k+l$ even. This makes it possible to deduce φ in all the boundary
584 layers from its form φ^{\pm} on the interior and exterior sides of the boundary layer of the
585 quarter-cell with centre at $(\pi/2, \pi/2)$.

586 We now obtain condition (4.6) governing the jump in φ at each corner. For definiteness,
587 let us consider the corner at $(0, 0)$ of the + quarter-cell with centre at $(\pi/2, \pi/2)$. Since

588 $-xy \sim \psi = O(\text{Pe}^{-1/2})$ near this corner, suitable rescaled coordinates are $\mathbf{X} = \text{Pe}^{1/4}\mathbf{x}$;
589 it terms of these, (2.4) reduces to

$$X\partial_X\phi - Y\partial_Y\phi + f\phi = 0 \quad (\text{B } 2)$$

590 to leading order in Pe. The solution is

$$\phi = X^{-f}\Phi(XY) \quad (\text{B } 3)$$

591 for some function Φ that is found by matching with the solution (4.3) valid away from
592 the corner. Upstream of the corner, this matching is made in the limit $Y \rightarrow \infty$ with
593 $XY = \zeta$ fixed; noting that $Y = \text{Pe}^{1/4}y \sim \text{Pe}^{1/4}(-2\sigma)^{1/2}$ and $H(\sigma) \sim \log(-\sigma/2)/2$, we
594 find

$$\Phi(\zeta) = (16\text{Pe})^{-f/4}\zeta^f \lim_{\sigma \rightarrow 0^-} \varphi(\sigma, \zeta). \quad (\text{B } 4)$$

595 Note that we retain the factor ζ^f although it is asymptotically small since $f \rightarrow 0$ as
596 $\text{Pe} \rightarrow \infty$. This is because this leads to logarithmic corrections to $f(\mathbf{q})$ which are not
597 negligible for large-but-finite Pe.

598 Downstream of the corner the analogous matching corresponds to the limit $X \sim$
599 $\text{Pe}^{1/4}(2\sigma)^{1/2} \rightarrow \infty$ with $XY = \zeta$ fixed and leads to

$$\Phi(\zeta) = (16\text{Pe})^{f/4} \lim_{\sigma \rightarrow 0^+} \varphi(\sigma, \zeta) \quad (\text{B } 5)$$

600 using that $H(\sigma) \sim \log(2/\sigma)/2$. Comparing (B 5) with (B 4) leads to the jump condition
601 (4.6) at $\sigma = 0$. The same condition applies to all corners.

602 We are now in position to write down the eigenvalue problem determining f . The heat
603 equation (4.5) makes it possible to relate the values of φ upstream of each corner to
604 that downstream of the preceding corner. Specifically, integrating the heat equation for
605 $0 < \sigma < 2$ gives

$$\varphi^+(2^-, \zeta) = \mathcal{H}_+\varphi^+(0^+, \zeta) + \mathcal{H}_-\varphi^-(0^+, \zeta), \quad (\text{B } 6)$$

$$\varphi^-(2^-, \zeta) = \mathcal{H}_-\varphi^+(0^+, \zeta) + \mathcal{H}_+\varphi^-(0^+, \zeta), \quad (\text{B } 7)$$

606 where \mathcal{H}_\pm are the linear operators giving the ‘time’-2 flow of the heat equation and are
607 defined by

$$(\mathcal{H}_\pm h)(\zeta) = \frac{1}{\sqrt{8\pi}} \int_0^\infty e^{-(\zeta \mp \zeta')^2/8} h(\zeta') d\zeta' \quad (\text{B } 8)$$

608 for any function $h(\zeta)$.

609 Relations analogous to (B 6) can be written down for $\varphi^\pm(4^-, \zeta)$, $\varphi^\pm(6^-, \zeta)$ and $\varphi^\pm(8^-, \zeta) =$
610 $\varphi^\pm(0^-, \zeta)$. The jump condition (4.6) can then be used to eliminate $\varphi^\pm(2k^-)$ in favour of
611 $\varphi^\pm(2k^+)$. For φ^+ , this is straightforward: (4.6) gives

$$\varphi^+(0^+, \zeta) = (16\text{Pe})^{-f/2}\zeta^f\varphi^+(0^-, \zeta)$$

612 and similar relations at the other 3 corners. For φ^- , this is somewhat more complicated:
613 because φ^- is defined in 4 different quarter-cells, the upstream profiles are not immedi-
614 ately available. The periodicity conditions(B 1) can however be used to express them in
615 terms of $\varphi^-(2k^-)$, see Figure 6. This leads to the jump conditions

$$\begin{aligned} \varphi^-(0^+, \zeta) &= (16\text{Pe})^{-f/2}e^{\pi(q_1+q_2)}\zeta^f\varphi^-(4^-, \zeta), & \varphi^-(2^+, \zeta) &= (16\text{Pe})^{-f/2}e^{\pi(q_2-q_1)}\zeta^f\varphi^-(6^-, \zeta), \\ \varphi^-(4^+, \zeta) &= (16\text{Pe})^{-f/2}e^{-\pi(q_1+q_2)}\zeta^f\varphi^-(0^-, \zeta), & \varphi^-(6^+, \zeta) &= (16\text{Pe})^{-f/2}e^{\pi(q_2-q_1)}\zeta^f\varphi^-(2^-, \zeta). \end{aligned}$$

616 Gathering these results, the eigenvalue problem can be written in the vector form (4.8)

617 where the linear operator \mathcal{L} is

$$\mathcal{L}(\mathbf{q}, \mathbf{f}) = \zeta^{\mathbf{f}} \begin{pmatrix} 0 & 0 & 0 & 0 & 0 & 0 & \mathcal{H}_+ & \mathcal{H}_- \\ 0 & 0 & ab\mathcal{H}_- & ab\mathcal{H}_+ & 0 & 0 & 0 & 0 \\ \mathcal{H}_+ & \mathcal{H}_- & 0 & 0 & 0 & 0 & 0 & 0 \\ 0 & 0 & 0 & 0 & a^{-1}b\mathcal{H}_- & a^{-1}b\mathcal{H}_+ & 0 & 0 \\ 0 & 0 & \mathcal{H}_+ & \mathcal{H}_- & 0 & 0 & 0 & 0 \\ 0 & 0 & 0 & 0 & 0 & 0 & (ab)^{-1}\mathcal{H}_- & (ab)^{-1}\mathcal{H}_+ \\ 0 & 0 & 0 & 0 & \mathcal{H}_+ & \mathcal{H}_- & 0 & 0 \\ ab^{-1}\mathcal{H}_- & ab^{-1}\mathcal{H}_+ & 0 & 0 & 0 & 0 & 0 & 0 \end{pmatrix}, \quad (\text{B 9})$$

618 with $a = e^{\pi q_1}$ and $b = e^{\pi q_2}$.

619 B.2. Asymptotic limits

620 In the limit $|\mathbf{q}| \ll 1$, the eigenvalue problem (4.9) or, equivalently, (4.2) can be solved
 621 by perturbation expansion in powers of $|\mathbf{q}|$. Since \mathbf{f} decreases rapidly with $|\mathbf{q}|$ (like $|\mathbf{q}|^4$
 622 as is verified below), the right-hand side of (4.2) and the jumps (4.6) are negligible.
 623 Expanding ϕ in powers of $|\mathbf{q}|$ then leads to the same sequence of equations (3.16)–(3.18)
 624 as considered in the $|\mathbf{q}| = O(\text{Pe}^{-1/4})$ regime. The solution is the same: to leading-order ϕ
 625 is a constant, and the slope of the solution as $\zeta \rightarrow \infty$ is related to this constant according
 626 to (3.19). This implies that

$$\frac{\partial \varphi}{\partial \zeta} \sim -\frac{\pi^2 \nu}{4} |\mathbf{q}|^2 \varphi \quad \text{as } \zeta \rightarrow \infty. \quad (\text{B 10})$$

627 This perturbative solution breaks down for large ζ , however, since the constant leading-
 628 order ϕ is inconsistent with the decay requirement for φ . For large ζ , the eigenfunction φ
 629 takes an exponential form:

$$\varphi \propto \exp(-\lambda \zeta) \quad \text{as } \zeta \rightarrow \infty$$

630 for some λ . Comparing with (B 10) gives

$$\lambda = \frac{\pi^2 \nu}{4} |\mathbf{q}|^2. \quad (\text{B 11})$$

631 It can be verified that the decay rate λ is related to the eigenvalue $\mu(\mathbf{q}, 0)$ by

$$\mu(\mathbf{q}, 0) = e^{2\lambda^2}. \quad (\text{B 12})$$

632 Combining (4.11), (B 11) and (B 12) yields the approximation (4.13).

633 For $|q_1|, |q_2| \gg 1$, the eigenvalue problem (4.9) simplifies dramatically. For definiteness,
 634 we assume $q_1, q_2 > 0$. In this case, $a^{-1}b^{-1} \ll 1 \ll ab$ in (B 9). This implies that φ_2 , the
 635 second component of φ , is its largest component, and that $\varphi_4 \ll \varphi_2 \ll \varphi_3$. Taking this
 636 into account reduces (4.9) to

$$\mu \begin{pmatrix} \varphi_2 \\ \varphi_3 \end{pmatrix} = \zeta^{\mathbf{f}} \begin{pmatrix} 0 & ab\mathcal{H}_- \\ \mathcal{H}_- & 0 \end{pmatrix} \begin{pmatrix} \varphi_2 \\ \varphi_3 \end{pmatrix},$$

637 and hence to

$$\mu^2 \varphi_2 = ab \zeta^{2\mathbf{f}} \mathcal{H}_-^2 \varphi_2.$$

638 Therefore, $\mu(\mathbf{q}, \mathbf{f}) = (ab)^{1/2} \hat{\mu}(\mathbf{f})$, where $\hat{\mu}(\mathbf{f})$ is the eigenvalue of $\zeta^{\mathbf{f}} \mathcal{H}_-$ and (4.14) follows.

- 639 Abel, M., Cencini, M., Vergni, D. & Vulpiani, A. 2002, Front speed enhancement in cellular
640 flows, *Chaos* **12**, 481–488.
- 641 Bensoussan, A., Lions, J. L. & Papanicolaou, G. C. 1989, *Asymptotic analysis of periodic struc-*
642 *tures*, Kluwer.
- 643 Childress, S. 1979, Alpha-effect in flux ropes and sheets, *Phys. Earth Planet. Int.* **20**, 172–180.
- 644 Childress, S. & Soward, A. M. 1989, Scalar transport and alpha-effect for a family of cat’s-eye
645 flows, *J. Fluid Mech.* **205**, 99–133.
- 646 Dembo, A. & Zeitouni, O. 1998, *Large deviations: techniques and applications*, Springer.
- 647 den Hollander, F. 2000, *Large deviations*, Fields Institute Monographs, American Mathematical
648 Society.
- 649 DLMF 2010, Digital library of mathematical functions, from <http://dlmf.nist.gov/>.
- 650 Ellis, R. S. 1995, An overview of the theory of large deviations and applications to statistical
651 physics, *Actuarial J.* **1**, 97–142.
- 652 Fannjiang, A. & Papanicolaou, G. 1994, Enhanced diffusion for periodic flows, *SIAM J. Appl.*
653 *Math.* **54**, 333–408.
- 654 Freidlin, M. 1985, *Functional integration and partial differential equations*, Princeton University
655 Press.
- 656 Freidlin, M. & Wentzell, A. 1994, *Random perturbations of Hamiltonian systems*, American
657 Mathematical Society.
- 658 Gärtner, J. & Freidlin, M. I. 1979, The propagation of concentration waves in periodic and
659 random media, *Soviet Math. Dokl.* **20**, 1282–1286.
- 660 Gorb, Y., Nam, D. & Novikov, A. 2011, Numerical simulations of diffusion in cellular flows at
661 high Péclet number, *Discrete Contin. Dyn. Syst. Ser. B* **15**, 75–92.
- 662 Haynes, P. H. & Vanneste, J. 2005, What controls the decay rate of passive scalars in smooth
663 random flows?, *Phys. Fluids* **17**, 097103.
- 664 Haynes, P. H. & Vanneste, J. 2014, Dispersion in the large-deviation regime. Part I: shear flows
665 and periodic flows, *J. Fluid Mech.* In press. Referred to as Part I.
- 666 Keller, J. B. 2004, Diffusion at finite speed and random walks, *Proc. Natl. Acad. Sci. USA*
667 **101**, 1120–1122.
- 668 Korolov, L. 2004, Random perturbations of two-dimensional Hamiltonian flows, *Prob. Theor.*
669 *Rel. Fields* **129**, 37–62.
- 670 Majda, A. J. & Kramer, P. R. 1999, Simplified models for turbulent diffusion: theory, numerical
671 modelling and physical phenomena, *Phys. Rep.* **314**, 237–574.
- 672 Moffatt, H. K. 1983, Transport effects associated with turbulence with particular attention to
673 the influence of helicity, *Rep. Prog. Phys.* **46**, 621–664.
- 674 Novikov, A. & Ryzhik, L. 2007, Boundary layers and KPP fronts in a cellular flow, *Arch. Rational*
675 *Mech. Anal.* **184**, 23–48.
- 676 Novikov, A., Papanicolaou, G. & Ryzhik, L. 2005, Boundary layers for cellular flows at high
677 Péclet numbers, *Comm. Pure Appl. Math.* **867–922**, 563–580.
- 678 Papanicolaou, G. C. 1995, Diffusion in random media, in J. P. Keller, ed., *Surveys in Applied*
679 *Mathematics*, Vol. 1, Plenum, pp. 205–253.
- 680 Pauls, W. 2006, Transport in cellular flows from the viewpoint of stochastic differential equations,
681 in O. Bühler & C. Doering, eds, *Proceedings of the 2005 Program on Geophysical Fluid*
682 *Dynamics*, Woods Hole Oceanographic Institution, pp. 144–156.
- 683 Rhines, P. B. & Young, W. R. 1983, How rapidly is a passive scalar mixed within closed stream-
684 lines, *J. Fluid Mech.* **133**, 133–145.
- 685 Rosenbluth, M. N., Berk, H. L., Dexas, I. & Horton, W. 1987, Effective diffusion in laminar
686 convective flows, *Phys. Fluids* **30**, 2636–2647.
- 687 Shraiman, B. I. 1987, Diffusive transport in a Rayleigh-Bénard convection cell, *Phys. Rev. A*
688 **36**, 261–267.
- 689 Soward, A. M. 1987, Fast dynamo action in a steady flow, *J. Fluid Mech.* **180**, 267–295.
- 690 Taylor, G. I. 1953, Dispersion of soluble matter in solvent flowing slowly through a tube, *Proc.*
691 *R. Soc. Lond. A* **219**, 186–203.
- 692 Touchette, H. 2009, Large deviation approach to statistical mechanics, *Phys. Rep.* **478**, 1–69.
- 693 Tsang, Y.-K., Antonsen, T. M. & Ott, E. 2005, Exponential decay of chaotically advected passive
694 scalars in the zero diffusivity limit, *Phys. Rev. E* **71**, 066301.

- 695 Tzella, A. & Vanneste, J. 2014*a*, Front propagation in cellular flows: a large-deviation approach.
696 In preparation.
- 697 Tzella, A. & Vanneste, J. 2014*b*, Front propagation in cellular flows for fast reaction and small
698 diffusivity. In preparation.
- 699 Xin, J. 2009, *An introduction to fronts in random media*, Springer.